Chapter 9
A Finite-Time Nonlinear PID Set-Point Controller for a Parallel Manipulator

Francisco Salas, Israel Soto, Raymundo Juarez and Israel U. Ponce

Abstract In recent years, finite-time controllers have attracted attention from some researchers in control, who have formulated applications to several processes and systems, including serial robotic manipulators. In this work, we report the application of a finite-time nonlinear PID controller to a Five-Bar Mechanism, which is a parallel manipulator, for set-point controller. The stability analysis of the closed-loop system shows global finite-time stability of the system. The dynamic model of the Five-Bar Mechanism developed in this work is a so-called reduced model, which has a structure similar to a serial robot. Moreover, the results of the numerical simulations carried out confirm the usefulness of the proposed application. The contribution of this work is to show the feasibility of the application of a finite-time nonlinear controller to a Five-Bar Mechanism and the usefulness of the proposed approach by numerical simulations.

Keywords Nonlinear controller · Finite-time PID · Parallel manipulator

9.1 Introduction

In recent years, finite-time controllers have attracted attention from some researchers in control.

As a result, the fundamental theory has been developed (Dorato 1961; Michel 1970; Weiss and Infante 1967) and enriched by many contributions (Bhat and Bernstein 1998, 2000, 2005; Polyakov and Poznyak 2009; Polyakov 2014). According to Amato et al. (2013), the finite-time stability is a property related to the quantitative behavior of the states of a system over a period of time.

F. Salas · R. Juarez
Universidad Autónoma de Coahuila, Facultad de Contaduría y Administración,
Blvd. Revolución 151 Oriente, Col. Centro, 27000 Torreón, Coahuila, CP, Mexico

I. Soto (✉) · I. U. Ponce
Universidad Autónoma de Ciudad Juárez, Instituto de Ingeniería
y Tecnología, Ciudad Juárez, Chihuahua, Mexico
e-mail: angel.soto@uacj.mx

O. O. Vergara Villegas et al. (eds.), *Advanced Topics on Computer Vision, Control and Robotics in Mechatronics*,
https://doi.org/10.1007/978-3-319-77770-2_9

A system is finite-time stable if, given a bound on an initial condition, the weighted norm of the state does not exceed a certain threshold over a specific time period. Moreover, finite-time stability and Lyapunov asymptotic stability are independent concepts, although not exclusively one from another. The existence of one does not imply the existence of the other. Some advantages of the finite-time stabilization of dynamic systems are that it can produce faster transient responses and high-precision performance, as well as convergence to the equilibrium in finite time. Some previous works in applications of finite-time controllers to robotic manipulators are Feng et al. (2002), Gruyitch and Kokosy (1999), Hong et al. (2002), Yu et al. (2005), Su and Zheng (2009, 2010), Zhao et al. (2010). In Su and Zheng (2009), a finite-time nonlinear PID-like control for regulation of robotic manipulators is presented. The authors propose a not model-based controller, to take advantage of the robustness to parametric uncertainty of the model. This work is improved in Su and Zheng (2010) by adding a nonlinear filter to estimate velocity when measurements are not available.

On the other hand, parallel robots are closed-chain mechanisms that possess some particular features such as high-speed capabilities and high stiffness that make them useful for some tasks as machining (Barnfather et al. 2017; Kelaiaia 2017), welding (Li et al. 2015; Wu et al. 2008), packaging (Pierrot et al. 1990; Xie and Liu 2016) as well as flight simulators (Huang and Cao 2005) and telescopes (Enferadi and Shahi 2016; Nan et al. 2011). Some recent approaches of control of this kind of robotic manipulators include not model-based controllers (Bourbonnais et al. 2015; Ren et al. 2007) and model-based controllers (Diaz-Rodriguez et al. 2013; Ren et al. 2007; Salinas et al. 2016). In Ren et al. (2007), a comparison of several control approaches for robot tracking of three degrees of freedom (DOF) parallel robot is presented. They compare the performance of an adaptive controller, a PI-type synchronized controller (model-based), a conventional PID controller, and an adaptive synchronized controller (not model-based). In Bourbonnais et al. (2015), a computed torque controller and a conventional PID controller are implemented for a novel Five-Bar parallel robot. In Diaz-Rodriguez et al. (2013), a reduced model-based controller of a three DOF parallel robot is proposed. The reduced model is obtained by considering a simplified model with a set of relevant parameters. In Salinas et al. (2016), a family of nonlinear PID-like controllers in which an integral action of a nonlinear function of the position error is added to the control signal.

In this work, inspired in the work of Su and Zheng (2017) on a finite-time controller for set-point controller of a serial robot, we propose the application of this controller to a parallel manipulator, in order to prove the finite-time stability of the closed-loop system by developing the stability analysis and to prove the feasibility and the usefulness of such an application. The dynamic model of the Five-Bar Mechanism constitutes a set of differential algebraic equations (DAEs). Based on Soto and Campa (2014) and Khan et al. (2005), a procedure is carried out in order to transform the set of DAEs into a set of ordinary differential equations (ODEs). By using such a model, the Lyapunov stability analysis and the finite-time stability analysis of the closed-loop system can be developed. As a result, the global

finite-time stability of the closed-loop system is proven. Moreover, such a model of ODEs representing the dynamics of the Five-Bar Mechanism let us to carry out numerical simulations of the system. The results of the simulations confirm the validity and usefulness of the application.

9.1.1 Mathematical Preliminaries

In this work, vectors are denoted with italic–bold lowercase letters, e.g., $\boldsymbol{x}$ or $\boldsymbol{\omega}$. Matrices are denoted with italic capital letters, e.g., $\boldsymbol{A}$. $\|\boldsymbol{x}\| = \sqrt{\boldsymbol{x}^T\boldsymbol{x}}$ represents the Euclidean norm of vector $\boldsymbol{x}$. $\lambda_{\max}\{A\}$ and $\lambda_{\min}\{A\}$ represent the largest and the smallest eigenvalues of matrix A, respectively.

In the following, based on Su and Zheng (2017) we define some useful vectors and vector functions, as well as a definition for the control design and analysis.

$$\mathrm{Sig}^{\alpha}(\boldsymbol{x}) = [|x_1|^{\alpha}\mathrm{sign}(x_1), \ldots, |x_n|^{\alpha}\mathrm{sign}(x_n)]^T \in \Re^n \tag{9.1}$$

$$\mathrm{Sech}(\boldsymbol{x}) = \mathrm{diag}(\mathrm{sech}(x_1), \ldots, \mathrm{sech}(x_n)) \in \Re^{n\times n} \tag{9.2}$$

where α_0 and α are positive constants, and $\boldsymbol{x} \in \Re^n$. Furthermore, $0<\alpha<1$, $\mathrm{sign}(\cdot)$, and $\mathrm{sech}(\cdot)$ are the standard scalar functions signum and hyperbolic secant, respectively, and $\mathrm{diag}(\cdot)$ denotes a diagonal matrix. By defining the vector function

$$\mathrm{Tanh}(\boldsymbol{x}) = [\tanh(x_1), \ldots, \tanh(x_n)]^T \in \Re^n, \tag{9.3}$$

the validity of the following expressions

$$\boldsymbol{x}^T\mathrm{Sig}^{\alpha}(\boldsymbol{x}) = \sum_{i=1}^{n} |x_i|^{\alpha+1} \geq \mathrm{Tanh}^T(\boldsymbol{x})\mathrm{Sig}^{\alpha}(\boldsymbol{x}) \geq 0 \tag{9.4}$$

$$|x_i|^{\alpha+1} \geq \tanh^2(x_i) \tag{9.5}$$

$$(\mathrm{Sech}^2(\boldsymbol{x}))_M = 1 \tag{9.6}$$

can be proven for all $\boldsymbol{x} \neq 0 \in \Re^n$.

9.1.2 Fundamentals of Finite-Time Stability Analysis

Although finite-time stability concepts in control systems literature can be traced back to decade of the 1960s, it was until the works reported in Bhat and Bernstein (1998) and (2000) when the foundations of finite-time stability theory were

rigorously established. In Bhat and Bernstein (2005) were further studied some conditions for finite-time stability, in relation to the homogeneity of a system. In the following, some definitions will be exposed in order to clarify the concepts of finite-time stability.

Definition 1 A function $V : \Re^n \to \Re$ is homogeneous of degree d with respect to the weights $\boldsymbol{p} = (p_1, \ldots, p_n) \in \Re^n$ if for any given $\delta > 0, V(\delta^{p_1} x_1, \ldots, \delta^{p_n} x_n) = \delta^d V(\boldsymbol{x}), \forall \boldsymbol{x} \in \Re^n$. A vector field $\boldsymbol{h}$ is homogeneous of degree d with respect to the weights $\boldsymbol{p} = (p_1, \ldots, p_n) \in \Re^n_+$, if for all $1 \leq i \leq n$, the ith component h_i is a homogeneous function of degree $p_i + d$.

Definition 2 Consider the system

$$\dot{\boldsymbol{x}} = \boldsymbol{h}(\boldsymbol{x}), \boldsymbol{h}(0) = 0, \boldsymbol{x} \in \Re^n \tag{9.7}$$

with $\boldsymbol{h} : U_0 \to \Re^n$ continuous on an open neighborhood U_0 of the origin. Suppose that system Eq. (9.1) possesses unique solutions in forward time for all initial condition. The equilibrium $\boldsymbol{x} = 0$ of system Eq. (9.1) is (locally) finite-time stable if it is Lyapunov stable and finite-time convergent in a neighborhood $U \subset U_0$ of the origin. The finite-time convergence means the existence of a function $T(\boldsymbol{x}_0) : U \backslash \{0\} \to (0, \infty)$, such that, $\forall \boldsymbol{x}_0 \in U \subset \Re^n$, the solution of Eq. (9.1) denoted by $s_t(\boldsymbol{x}_0)$ with $\boldsymbol{x}_0$ as the initial condition is defined and $s_t(\boldsymbol{x}_0) \in U \backslash \{0\}$ for $t \in [0, T(\boldsymbol{x}_0))$ and $\lim_{t \to T(\boldsymbol{x}_0)} s_t(\boldsymbol{x}_0) = 0$. When $U = \Re^n$, the global finite-time stability is obtained.

Remark 1 The system (7) is homogeneous if $\boldsymbol{h}(\cdot)$ is homogeneous.

The following results represent sufficient conditions for finite-time stability of the closed-loop system.

Lemma 1 (Hong et al. 2002; Huang and Cao 2005)
Consider the system

$$\dot{\boldsymbol{x}} = \boldsymbol{h}(\boldsymbol{x}) + \hat{\boldsymbol{h}}(\boldsymbol{x}), \boldsymbol{h}(0) = 0, \hat{\boldsymbol{h}}(0) = 0, \boldsymbol{x} \in \Re^n \tag{9.8}$$

where $\boldsymbol{h}(\boldsymbol{x})$ is a continuous homogeneous vector field of degree $d < 0$, with respect to $(p_1, \ldots, p_n)$. Assume that $\boldsymbol{x} = 0$ is an asymptotically stable equilibrium of system Eq. (9.7). *Then, $\boldsymbol{x} = 0$ is a locally finite-time stable equilibrium of system* Eq. (9.8) if

$$\lim_{\delta \to 0} \frac{\hat{f}_i(\delta^{p_1} x_1, \ldots, \delta^{p_n} x_n)}{\delta^{d + p_i}} = 0, \; i = 1, \ldots, n, \forall \boldsymbol{x} \neq 0 \tag{9.9}$$

Lemma 2 (Hong et al. 2002; Su and Zheng (2017)
Global asymptotical stability and finite-time stability imply global finite-time stability.

9.2 Dynamic Model of a Parallel Robot Manipulator

A parallel robot manipulator is a closed-chain mechanism (CCM) that consists of kinematic chains which are connected in loops. Consider a CCM with n actuated joints. Due to its closed configuration, the CCM is subject to holonomic constraints. In this work, the actuated joints are represented by the vector $\boldsymbol{q} \in \Re^n$, while the non-actuated joints are represented by the vector $\boldsymbol{\beta} \in \Re^m$ and the holonomic constraints are represented by the vector $\boldsymbol{\gamma} \in \Re^r$. Let us define the vector of generalized coordinates $\boldsymbol{\rho}$ that fully explicitly represents the configuration of the CCM as

$$\boldsymbol{\rho} = \left[\boldsymbol{q}^T \boldsymbol{\beta}^T\right]^T \in \Re^s$$

with $s = n + m$. By applying the Euler–Lagrange formulation, the dynamic model of a parallel robot with viscous friction is in general formulated as

$$\begin{aligned} &M'(\boldsymbol{\rho})\ddot{\boldsymbol{\rho}} + C'(\boldsymbol{\rho}, \dot{\boldsymbol{\rho}})\dot{\boldsymbol{\rho}} + \mathbf{g}'(\boldsymbol{\rho}) + F'\dot{\boldsymbol{\rho}} = \boldsymbol{\tau}' + D^T(\boldsymbol{\rho})\boldsymbol{\lambda} \\ &\boldsymbol{\gamma}(\boldsymbol{\rho}) = 0 \end{aligned} \tag{9.10}$$

where $M'(\boldsymbol{\rho}) \in \Re^{s\times s}$ represents the inertia matrix, $C'(\boldsymbol{\rho}, \dot{\boldsymbol{\rho}}) \in \Re^{s\times s}$ is the matrix of terms arising from the centripetal and Coriolis forces, $\boldsymbol{g}'(\boldsymbol{\rho}) \in \Re^s$ represents the vector of forces due to gravity, $F' \in \Re^{s\times s}$ represents the diagonal matrix of viscous friction coefficients, $\boldsymbol{\tau}' \in R^s$ is the vector of generalized forces associated with scalar variables of $\boldsymbol{\rho}, D(\boldsymbol{\rho}) = \frac{\partial \gamma(\rho)}{\partial \boldsymbol{\rho}} \in \Re^{r\times s}$ is the Jacobian matrix of the system holonomic constraints $\boldsymbol{\gamma}(\boldsymbol{\rho}) \in \Re^r$, or the constraint Jacobian, and $\boldsymbol{\lambda} \in \Re^r$ is the vector of Lagrange multipliers.

Notice that Eq. (9.1) constitutes a set of DAEs. There are several methods to transform the DAEs into ODEs (Khan et al. 2005; Soto and Campa 2014). The purpose of such a transformation is to be able to apply standard numerical methods for solving the ODEs rather than the DAEs. One of the most important methods is the method of projection via the constraint Jacobian. According to Soto and Campa (2014, 2015), this method consists of finding a matrix $R(\boldsymbol{\rho})$ whose column space belongs to the null space of $D(\boldsymbol{\rho})$, i.e., $D(\boldsymbol{\rho})R(\boldsymbol{\rho}) = 0$. By considering $\dot{\boldsymbol{q}} = \mathrm{d}\boldsymbol{q}/\mathrm{d}t$ as the vector of independent velocities and $\dot{\boldsymbol{\rho}} = \mathrm{d}\boldsymbol{\rho}/\mathrm{d}t$ as the vector of feasible dependent velocities of a constrained body that belong to the space spanned by the columns of $R(\boldsymbol{\rho})$, we obtain the expression

$$\dot{\boldsymbol{\rho}} = R(\boldsymbol{\rho})\dot{\boldsymbol{q}} \tag{9.11}$$

with $R(\boldsymbol{\rho}) \in \Re^{s\times n}$. Notice that, given the differential kinematic model $\dot{\boldsymbol{\beta}} = J_\beta(\boldsymbol{\rho})\dot{\boldsymbol{q}}$, the matrix $R(\boldsymbol{\rho})$ can be constructed as

$$R(\boldsymbol{\rho}) = \begin{bmatrix} I_n \\ J_\beta(\boldsymbol{\rho}) \end{bmatrix} \tag{9.12}$$

where I_n is the identity matrix of dimensions $n \times n$. It can be proven that, by substituting the expression in Eq. (9.11) and its temporal derivative in model Eq. (9.10), it can be written as

$$M(\boldsymbol{\rho})\boldsymbol{q} + C(\boldsymbol{\rho}, \dot{\boldsymbol{\rho}})\dot{\boldsymbol{q}} + \boldsymbol{g}(\boldsymbol{\rho}) + F\dot{\boldsymbol{q}} = \boldsymbol{\tau} \tag{9.13}$$

where

$$M(\boldsymbol{\rho}) = R^T(\boldsymbol{\rho})M'(\boldsymbol{\rho})R(\boldsymbol{\rho}) \tag{9.14}$$

$$C(\boldsymbol{\rho}, \dot{\boldsymbol{\rho}}) = R^T(\boldsymbol{\rho})M'(\boldsymbol{\rho})\dot{R}(\boldsymbol{\rho}) + R^T(\boldsymbol{\rho})C'(\boldsymbol{\rho}, \dot{\boldsymbol{\rho}})R(\boldsymbol{\rho}) \tag{9.15}$$

$$\boldsymbol{g}(\boldsymbol{\rho}) = R^T(\boldsymbol{\rho})\boldsymbol{g}'(\boldsymbol{\rho}) \tag{9.16}$$

$$F = R^T(\boldsymbol{\rho})F'R(\boldsymbol{\rho}) \tag{9.17}$$

$$\boldsymbol{\tau} = R^T(\boldsymbol{\rho})\boldsymbol{\tau}' \tag{9.18}$$

Notice that the term of Eq. (9.10) containing the product of the constraint Jacobian by the Lagrange multipliers vanishes because it belongs to the null space of $R(\boldsymbol{\rho})$, as it was pointed above.

Ghorbel et al. (2000) proven that there exist a unique parametrization $\boldsymbol{\rho} = \boldsymbol{\eta}(\boldsymbol{q})$ of $\boldsymbol{\rho} \in N_\rho$ inside a neighborhood N_ρ, whenever the system is not in a singular configuration. Moreover, Muller (2005) established that, for a parallel machine, a subset $\boldsymbol{q}$ of $\boldsymbol{n}$ joint variables determines its configuration, in virtue of that exist a smooth mapping φ that assigns to each $\boldsymbol{\rho}$ the parallel machine configuration as $\boldsymbol{\rho} = \varphi(\boldsymbol{q})$, where the map φ^{-1} is a local parametrization of the n dimensional manifold V, such as $V = \{\boldsymbol{\rho} \in V^n; \boldsymbol{\gamma}(\boldsymbol{\rho}) = 0\}$, where V represents the set of all admissible configurations of the parallel machine, and $\boldsymbol{\gamma}(\boldsymbol{\rho}) = 0$ represents the holonomic constraints.

In consequence, we can write down, without loss of generality, the matrices and vectors of the dynamic model $M(\boldsymbol{\rho})$, $C(\boldsymbol{\rho}, \dot{\boldsymbol{\rho}})$ and $g(\boldsymbol{\rho})$ as $M(\boldsymbol{q})$, $C(\boldsymbol{q}, \dot{\boldsymbol{q}})$ and $g(\boldsymbol{q})$, respectively. Thus, the dynamic model Eq. (9.10) takes the form

$$M(\boldsymbol{q})\boldsymbol{q} + C(\boldsymbol{q}, \dot{\boldsymbol{q}})\dot{\boldsymbol{q}} + \boldsymbol{g}(\boldsymbol{q}) + F\dot{\boldsymbol{q}} = \boldsymbol{\tau} \tag{9.19}$$

The model Eq. (9.19) exhibits the following properties.

Property 1 Cheng et al. 2003

The inertia matrix $M(\boldsymbol{q})$ is symmetric and positive definite.

Property 2 *The inertia matrix $M(\boldsymbol{q})$ is bounded as*

$$\|M(\boldsymbol{q})\| \leq M_M$$

where M_M is a positive finite constant, whenever the robot is not in singular configuration.

Proof Since $\|A^T B\| \leq \|A\|\|B\|$, from Eq. (9.14) we can write

$$\left\|R^T M' R\right\| \leq \left\|R^T\right\|\|M'\|\|R\|$$

Norm $\|M'\|$ is upper bounded whenever its entries are finite. For robots with only revolute joints, this is assured because entries of matrix M' are sinusoidal functions of joint variables with constant coefficients. On the other hand, $\|R\|$ is upper bounded whenever its entries are finite, that is to say, matrix $\|R\|$ is well posed. From Eq. (9.12) it can be noticed that $\|R\|$ is well posed whenever there exists a continuous mapping between $\dot{\boldsymbol{\rho}}$ and $\dot{\boldsymbol{q}}$; i.e., the robot is not in singular configuration.

Property 3 (Ghorbel et al. 2000; Cheng et al. 2003)
The matrix $\frac{1}{2}\dot{M}(\boldsymbol{q}) - C(\boldsymbol{q}, \dot{\boldsymbol{q}})$ is skew-symmetric.

Property 4 (Khalil and Dombre 2004)
There exists a constant $k_C > 0$ such that $\|C_r(\boldsymbol{q}, \dot{\boldsymbol{q}})\| \leq k_C\|\dot{\boldsymbol{q}}\|$, for all $\boldsymbol{q} \in \Re^n$.

Property 5 *The friction matrix F can be bounded as*

$$f_m I \leq F \leq f_M I$$

9.3 Finite-Time Nonlinear PID Controller

The solution of the problem of global finite-time regulation of a robot manipulator implies finding input torques for the actuators of the manipulator in order to reach a desired position $\boldsymbol{q}_d$, such that for any initial state $(\boldsymbol{q}(0), \dot{\boldsymbol{q}}(0))$, $\tilde{\boldsymbol{q}} = \boldsymbol{q} - \boldsymbol{q}_d \to 0$ and $\dot{\boldsymbol{q}}(t) \to 0$ in finite time.

In this work, we propose to apply the finite-time regulation controller, inspired in Su and Zheng (2017)

$$\boldsymbol{\tau} = -K_p \operatorname{Sig}^{\alpha_1}(\tilde{\boldsymbol{q}}) - K_d \operatorname{Sig}^{\alpha 2}(\boldsymbol{\eta}) - k_{p0} - K_I \int_0^t \boldsymbol{\eta}(\sigma)\, \mathrm{d}\sigma - k_{d0}\dot{\boldsymbol{q}} \tag{9.20}$$

to a CCM, with

$$\eta = \dot{\boldsymbol{q}} + \alpha_0 \tanh(\tilde{\boldsymbol{q}}) \tag{9.21}$$

and

$$\varphi = \int_0^t \boldsymbol{\eta}(\sigma)\, \mathrm{d}\sigma \tag{9.22}$$

K_p, K_I and K_d are positive definite constant diagonal control gain matrices, respectively; k_{p0} and k_{d0} are positive constants and $0<\alpha_1<1$, while $\alpha_2 = 2\alpha_1/(\alpha_1+1)$. By substituting Eqs. (9.20) and (9.22) in Eq. (9.19), we obtain

$$\begin{aligned} &M(\boldsymbol{q})\ddot{\boldsymbol{q}} + C(\boldsymbol{q},\dot{\boldsymbol{q}})\dot{\boldsymbol{q}} + F\dot{\boldsymbol{q}} \\ &\quad + K_p\,\mathrm{Sig}^{\alpha_1}(\tilde{\boldsymbol{q}}) + K_d\,\mathrm{Sig}^{\alpha_2}(\boldsymbol{\eta}) + k_{p0}\tilde{\boldsymbol{q}} + k_{d0}\dot{\boldsymbol{q}} + K_I\varphi = 0 \end{aligned} \tag{9.23}$$

With Eqs. (9.22) and (9.23), and taking into account that $\dot{\tilde{\boldsymbol{q}}} = \dot{\boldsymbol{q}}$ when $\boldsymbol{q}_d = 0$, the closed-loop equation can be written as

$$\frac{\mathrm{d}}{\mathrm{d}t}\begin{bmatrix}\tilde{\boldsymbol{q}}\\ \dot{\boldsymbol{q}}\\ \varphi\end{bmatrix} = \begin{bmatrix} \dot{\boldsymbol{q}} \\ -M^{-1}(\boldsymbol{q})[C(\boldsymbol{q},\dot{\boldsymbol{q}})\dot{\boldsymbol{q}} + F\dot{\boldsymbol{q}} + K_p\,\mathrm{Sig}^{\alpha_1}(\tilde{\boldsymbol{q}}) + K_d\,\mathrm{Sig}^{\alpha_2}(\boldsymbol{\eta}) \\ \quad + K_I\varphi + k_{p0}\tilde{\boldsymbol{q}} + k_{d0}\dot{\boldsymbol{q}}] \\ \dot{\boldsymbol{q}} + \alpha_0\,\mathrm{Tanh}(\tilde{\boldsymbol{q}}) \end{bmatrix} \tag{9.24}$$

Notice that the origin of the system Eq. (9.24) is the only equilibrium of the system.

9.3.1 Stability Analysis of the Closed-Loop System

By proceeding inspired in Su and Zheng (2017), we study the global asymptotical stability of Eq. (9.24). First, we propose the Lyapunov function candidate

$$\begin{aligned} V(\tilde{\boldsymbol{q}},\dot{\boldsymbol{q}},\varphi) = &\frac{1}{2}\dot{\boldsymbol{q}}^T M(\boldsymbol{q})\dot{\boldsymbol{q}} + \alpha_0\,\mathrm{Tanh}^T(\tilde{\boldsymbol{q}})M(\boldsymbol{q})\dot{\boldsymbol{q}} + \frac{1}{2}k_{p0}\tilde{\boldsymbol{q}}^T\tilde{\boldsymbol{q}} \\ &+ \frac{1}{\alpha_1+1}\sum_{i=1}^{n} k_{pi}|\tilde{q}_i|^{\alpha_1+1} + \alpha_0\sum_{i=1}^{n}(f_i + k_{d0})\ln(\cosh(\tilde{q}_i)) + \frac{1}{2}\varphi^T K_I\varphi \end{aligned} \tag{9.25}$$

where f_i is the ith entry of friction matrix F. In order to investigate positive definiteness of Eq. (9.25), notice that in virtue of

$$\begin{aligned} &\frac{1}{4}\dot{\boldsymbol{q}}^T M(\boldsymbol{q})\dot{\boldsymbol{q}} + \alpha_0\,\mathrm{Tanh}^T(\tilde{\boldsymbol{q}})M(\boldsymbol{q})\dot{\boldsymbol{q}} + \frac{1}{2(\alpha_1+1)}\sum_{i=1}^{n} k_{pi}|\tilde{q}_i|^{\alpha_1+1} \\ &\quad \geq \frac{1}{2(\alpha_1+1)}\sum_{i=1}^{n}\left[k_{pi} - 2(\alpha_1+1)\alpha_0^2 M_M\right]\tanh^2(\tilde{q}_i) \end{aligned}$$

where we have used Property 2 and Eq. (9.5), we can lower bound Eq. (9.25) as

$$V \geq \frac{1}{2(\alpha_1+1)} \sum_{i=1}^{n} \left[k_{pi} - 2(\alpha_1+1)\alpha_0^2 M_M\right] \tanh^2(\tilde{q}_i) + \frac{1}{2} k_{p0} \tilde{\boldsymbol{q}}^T \tilde{\boldsymbol{q}} + \frac{1}{2} \varphi^T K_I \varphi + \frac{1}{4} \dot{\boldsymbol{q}}^T M(\boldsymbol{q}) \dot{\boldsymbol{q}} + \alpha_0 \sum_{i=1}^{n} (f_i + k_{d0}) \ln(\cosh(\tilde{q}_i)) \tag{9.26}$$

The three last terms of the right side of inequality Eq. (9.26) can be lower bounded as

$$\begin{aligned} &\frac{1}{2} \varphi^T K_I \varphi \geq \frac{1}{2} \lambda_{\min}\{K_I\} \|\varphi\|^2 > 0, \forall \varphi \neq 0 \in \Re^n \\ &\frac{1}{4} \dot{\boldsymbol{q}}^T M(\boldsymbol{q}) \dot{\boldsymbol{q}} \geq \frac{1}{4} \lambda_{\min}\{M(\boldsymbol{q})\} \|\dot{\boldsymbol{q}}\|^2 > 0, \forall \dot{\boldsymbol{q}} \neq 0 \in \Re^n \\ &\alpha_0 \sum_{i=1}^{n} (f_i + k_{d0}) \ln(\cosh(\tilde{q}_i)) \geq \alpha_0 \sum_{i=1}^{n} (f_i + k_{d0}) \mathrm{e} > 0 \end{aligned}$$

The second term of the right side of inequality Eq. (9.26) is positive definite since $\frac{1}{2} k_{p0} \tilde{\boldsymbol{q}}^T \tilde{\boldsymbol{q}} = \frac{1}{2} k_{p0} \|\tilde{\boldsymbol{q}}\|^2$. Notice that the first term or the right side of Eq. (9.26) is positive as long as $k_{pi} - 2(\alpha_1+1)\alpha_0^2 M_M$ is positive, i.e.,

$$k_{pi} > 2(\alpha_1+1)\alpha_0^2 M_M \tag{9.27}$$

Therefore, since the fourth last terms of the right side of Eq. (9.26) are positive definite for all $\tilde{\boldsymbol{q}}, \dot{\boldsymbol{q}}, \varphi \neq 0 \in \Re^n$, the Lyapunov candidate function Eq. (9.25) is positive definite while Eq. (9.27) is satisfied.

The temporal derivative of the Lyapunov function candidate Eq. (9.25) is as follows:

$$\begin{aligned} \dot{V}(\tilde{\boldsymbol{q}}, \dot{\boldsymbol{q}}, \varphi) = &\frac{1}{2} \dot{\boldsymbol{q}}^T \dot{M}(\boldsymbol{q}) \dot{\boldsymbol{q}} + \dot{\boldsymbol{q}}^T M(\boldsymbol{q}) \ddot{\boldsymbol{q}} + \alpha_0 (\mathrm{Sech}^2(\tilde{\boldsymbol{q}}) \dot{\tilde{\boldsymbol{q}}})^T M(\boldsymbol{q}) \dot{\boldsymbol{q}} \\ &+ \alpha_0 \mathrm{Tanh}^T(\tilde{\boldsymbol{q}}) \dot{M}(\boldsymbol{q}) \dot{\boldsymbol{q}} + \alpha_0 \mathrm{Tanh}^T(\tilde{\boldsymbol{q}}) M(\boldsymbol{q}) \ddot{\boldsymbol{q}} + k_{p0} \dot{\tilde{\boldsymbol{q}}}^T \tilde{\boldsymbol{q}} \\ &+ \dot{\tilde{\boldsymbol{q}}}^T K_p \, \mathrm{Sig}^{\alpha_1}(\tilde{\boldsymbol{q}}) + \alpha_0 \mathrm{Tanh}^T(\tilde{\boldsymbol{q}}) (F + k_{d0} I) \dot{\tilde{\boldsymbol{q}}} + \dot{\varphi}^T K_I \varphi \end{aligned} \tag{9.28}$$

Along the trajectories of the closed-loop system in Eq. (9.24), we obtain

$$\begin{aligned} \dot{V} = &-\dot{\boldsymbol{q}}^T F \dot{\boldsymbol{q}} - k_{d0} \dot{\boldsymbol{q}}^T \dot{\boldsymbol{q}} - \alpha_0 \mathrm{Tanh}(\tilde{\boldsymbol{q}}) K_p \, \mathrm{Sig}^{\alpha_1}(\tilde{\boldsymbol{q}}) - \boldsymbol{\eta}^T K_d \, \mathrm{Sig}^{\alpha_2}(\boldsymbol{\eta}) \\ &+ \alpha_0 [\mathrm{Tanh}(\tilde{\boldsymbol{q}}) C(\boldsymbol{q}, \dot{\boldsymbol{q}}) \dot{\boldsymbol{q}} + (\mathrm{Sech}^2(\tilde{\boldsymbol{q}}) \dot{\boldsymbol{q}})^T M(\boldsymbol{q}) \dot{\boldsymbol{q}}] - \alpha_0 \mathrm{k_{p0}} \mathrm{Tanh}(\tilde{\boldsymbol{q}}) \tilde{\boldsymbol{q}} \end{aligned} \tag{9.29}$$

where we have used the Property 3 (skew symmetry). Here, we neglect the gravitational forces vector from Eq. (9.24) since the CCM is a horizontal Five-Bar

Mechanism, in which motion of interest is not subject to gravitational forces. The two parts of the fifth term of the right side of Eq. (9.29) can be upper bounded as

$$\begin{aligned}\text{Tanh}(\tilde{\boldsymbol{q}})C(\boldsymbol{q},\dot{\boldsymbol{q}})\dot{\boldsymbol{q}} &\leq \|\text{Tanh}(\tilde{\boldsymbol{q}})C(\boldsymbol{q},\dot{\boldsymbol{q}})\dot{\boldsymbol{q}}\| \\ &\leq \|\text{Tanh}(\tilde{\boldsymbol{q}})\|\|C(\boldsymbol{q},\dot{\boldsymbol{q}})\|\|\dot{\boldsymbol{q}}\| \\ &\leq \sqrt{n}k_C\|\dot{\boldsymbol{q}}\|^2 \\ (\text{Sech}^2(\tilde{\boldsymbol{q}})\dot{\boldsymbol{q}})^T M(\boldsymbol{q})\dot{\boldsymbol{q}} &\leq \left\|(\text{Sech}^2(\tilde{\boldsymbol{q}})\dot{\boldsymbol{q}})^T M(\boldsymbol{q})\dot{\boldsymbol{q}}\right\| \\ &\leq \left\|(\text{Sech}^2(\tilde{\boldsymbol{q}})\dot{\boldsymbol{q}})^T\right\|\|M(\boldsymbol{q})\|\|\dot{\boldsymbol{q}}\| \\ &\leq M_M\|\dot{\boldsymbol{q}}\|^2\end{aligned}$$

where we have used Eq. (9.2), Property 2, and Property 4. Thus, the fifth term of the right side of Eq. (9.29) can be upper bounded as

$$\begin{aligned}&\alpha_0[\text{Tanh}(\tilde{\boldsymbol{q}})C(\boldsymbol{q},\dot{\boldsymbol{q}})\dot{\boldsymbol{q}} + (\text{Sech}^2(\tilde{\boldsymbol{q}})\dot{\boldsymbol{q}})^T M(\boldsymbol{q})\dot{\boldsymbol{q}}] \\ &\quad\leq \alpha_0(\sqrt{n}k_C + M_M)\|\dot{\boldsymbol{q}}\|^2\end{aligned} \tag{9.30}$$

In addition, by using Property 5 the first term of the right side of Eq. (9.29) can be upper bounded as

$$-\dot{\boldsymbol{q}}^T F\dot{\boldsymbol{q}} \leq -f_m\|\dot{\boldsymbol{q}}\|^2 \tag{9.31}$$

After substituting Eqs. (9.30) and (9.31) in Eq. (9.29) and rearranging terms, we can upper bound Eq. (9.29) as

$$\begin{aligned}\dot{V} \leq &-\left[f_m + k_{d0} - \alpha_0\left(\sqrt{n}k_C + M_M\right)\right]\|\dot{\boldsymbol{q}}\|^2 - \alpha_0\text{Tanh}\,(\tilde{\boldsymbol{q}})K_p\,\text{Sig}^{\alpha_1}(\tilde{\boldsymbol{q}}) \\ &-\boldsymbol{\eta}^T K_d\,\text{Sig}^{\alpha_2}(\boldsymbol{\eta}) - \alpha_0 \text{k}_{\text{p0}}\text{Tanh}(\tilde{\boldsymbol{q}})\tilde{\boldsymbol{q}}\end{aligned}$$

In virtue of that, $\tanh(\boldsymbol{x})$ and $\boldsymbol{x}$ have the same sign, and then $\text{Tanh}(\tilde{\boldsymbol{q}})\tilde{\boldsymbol{q}} > 0, \forall\tilde{\boldsymbol{q}} \neq 0$. Therefore, we can write

$$\begin{aligned}\dot{V} \leq &-\left[f_m + k_{d0} - \alpha_0\left(\sqrt{n}k_C + M_M\right)\right]\|\dot{\boldsymbol{q}}\|^2 - \alpha_0\text{Tanh}(\tilde{\boldsymbol{q}})K_p\,\text{Sig}^{\alpha_1}(\tilde{\boldsymbol{q}}) \\ &-\boldsymbol{\eta}^T K_d\,\text{Sig}^{\alpha_2}(\boldsymbol{\eta})\end{aligned} \tag{9.32}$$

After using the expression in Eq. (9.4), Eq. (9.32) can be rewritten as

$$\begin{aligned}\dot{V} \leq &-\left[f_m + k_{d0} - \alpha_0\left(\sqrt{n}k_C + M_M\right)\right]\|\dot{\boldsymbol{q}}\|^2 - \alpha_0\sum_{i=1}^{n} k_{pi}|\tanh(\tilde{q}_i)||\tilde{q}_i|^{\alpha_1} \\ &-\sum_{i=1}^{n} k_{di}|\eta_i|^{\alpha_2+1}\end{aligned} \tag{9.33}$$

where k_{pi} and k_{di} represent the ith diagonal elements of matrices K_p and K_d, respectively. Therefore, we can conclude that $\dot{V} \leq 0$ as long as

$$k_{d0} > \alpha_0(\sqrt{n}k_C + M_M) - f_m \tag{9.34}$$

is satisfied. In order to conclude the global asymptotical stability of the closed-loop system Eq. (9.24), by LaSalle's theorem (Kelly et al. 2005), we have that $\tilde{\boldsymbol{q}}(t) \to 0$, $\dot{\boldsymbol{q}}(t) \to 0$ and $\varphi(t) \to 0$ when $t \to \infty$ for any initial state. Thus, we conclude the global asymptotical stability of origin of the closed-loop system Eq. (9.24).

9.3.2 Finite-Time Stability

In this section, we will apply the concepts of finite-time stability in order to establish, in a similar way to Su and Zheng (2017), the stability of the closed-loop system in finite time. We first define the state vector $\boldsymbol{y} = \begin{bmatrix} \boldsymbol{y}_1^T & \boldsymbol{y}_2^T & \boldsymbol{y}_3^T \end{bmatrix}^T$ where $\boldsymbol{y}_1 = \tilde{\boldsymbol{q}}$, $\boldsymbol{y}_2 = \boldsymbol{\eta}$ and $\boldsymbol{y}_3 = \varphi$. The closed-loop system of state vector $\boldsymbol{y}$ can be written as

$$\frac{\mathrm{d}}{\mathrm{d}t}\begin{bmatrix} \boldsymbol{y}_1 \\ \boldsymbol{y}_2 \\ \boldsymbol{y}_3 \end{bmatrix} = \begin{bmatrix} \boldsymbol{y}_2 - \alpha_0 \mathrm{Tanh}(\boldsymbol{y}_1) \\ -\mathrm{M}^{-1}(\boldsymbol{y}_1 + \boldsymbol{q}_d)[(C(\boldsymbol{y}_1 + \boldsymbol{q}_d, \boldsymbol{y}_2 - \alpha_0 \mathrm{Tanh}(\boldsymbol{y}_1)) \\ + F + k_{d0}\boldsymbol{I})(\boldsymbol{y}_2 - \alpha_0 \mathrm{Tanh}(\boldsymbol{y}_1)) + K_p \mathrm{Sig}^{\alpha_1}(\boldsymbol{y}_1) \\ + K_d \mathrm{Sig}^{\alpha_2}(\boldsymbol{y}_2) + k_{p0}\boldsymbol{y}_1 + K_I \boldsymbol{y}_3] \\ + \alpha_0(\mathrm{Sech}^2(\boldsymbol{y}_1)(\boldsymbol{y}_2 - \alpha_0 \mathrm{Tanh}(\boldsymbol{y}_1))) \\ \boldsymbol{y}_2 \end{bmatrix} \tag{9.35}$$

Notice that the origin $\boldsymbol{y} = 0 \in \Re^{3n}$ is the equilibrium of Eq. (9.35). Equation (9.35) can be rewritten as

$$\frac{\mathrm{d}}{\mathrm{d}t}\begin{bmatrix} \boldsymbol{y}_1 \\ \boldsymbol{y}_2 \\ \boldsymbol{y}_3 \end{bmatrix} = \begin{bmatrix} \boldsymbol{y}_2 + \hat{\boldsymbol{h}}_1(y) \\ -\mathrm{M}^{-1}(\boldsymbol{q}_d)\left[K_p \mathrm{Sig}^{\alpha_1}(\boldsymbol{y}_1) + K_d \mathrm{Sig}^{\alpha_2}(\boldsymbol{y}_2)\right] + \hat{\boldsymbol{h}}_2(y) \\ \boldsymbol{y}_2 \end{bmatrix} \tag{9.36}$$

where

$$\hat{\boldsymbol{h}}_1 = -\alpha_0 \mathrm{Tanh}(\boldsymbol{y}_1) \tag{9.37}$$

$$\begin{aligned} \hat{\boldsymbol{h}}_2 = & -M^{-1}(\boldsymbol{y}_1 + \boldsymbol{q}_d)[(C(\boldsymbol{y}_1 + \boldsymbol{q}_d, \boldsymbol{y}_2 - \alpha_0 \mathrm{Tanh}(\boldsymbol{y}_1)) \\ & + F + k_{d0}\boldsymbol{I})(\boldsymbol{y}_2 - \alpha_0 \mathrm{Tanh}(\boldsymbol{y}_1)) + k_{p0}\boldsymbol{y}_1 + K_I(\boldsymbol{y}_3)\boldsymbol{y}_3] \\ & - \widetilde{M}(\boldsymbol{y}_1, \boldsymbol{q}_d)[K_p \mathrm{Sig}^{\alpha_1}(\boldsymbol{y}_1) + K_d \mathrm{Sig}^{\alpha_2}(\boldsymbol{y}_2)] \\ & + \alpha_0(\mathrm{Sech}^2(\boldsymbol{y}_1)(\boldsymbol{y}_2 - \alpha_0 \mathrm{Tanh}(\boldsymbol{y}_1))) \end{aligned} \tag{9.38}$$

$$\widetilde{M}(\boldsymbol{y}_1, \boldsymbol{q}_d) = -M^{-1}(\boldsymbol{y}_1 + \boldsymbol{q}_d) - M^{-1}(\boldsymbol{y}_1 + \boldsymbol{q}_d) \tag{9.39}$$

Now consider the closed-loop system

$$\frac{\mathrm{d}}{\mathrm{d}t}\begin{bmatrix}\boldsymbol{y}_1\\ \boldsymbol{y}_2\\ \boldsymbol{y}_3\end{bmatrix} = \begin{bmatrix}\boldsymbol{y}_2\\ -\mathrm{M}^{-1}(\boldsymbol{q}_d)\left[K_p\,\mathrm{Sig}^{\alpha_1}(\boldsymbol{y}_1) + K_d\,\mathrm{Sig}^{\alpha_2}(\boldsymbol{y}_2)\right]\\ \boldsymbol{y}_2\end{bmatrix} \tag{9.40}$$

which, according to Definition 1, is homogeneous if the following expressions are satisfied:

$$\begin{aligned} p_2 &= d + p_1\\ \alpha_1 p_1 &= \alpha_2 p_2 = d + p_2\\ p_2 &= d + p_3 \end{aligned} \tag{9.41}$$

It can be verified that with the values $p_1 = 2$, $p_2 = \alpha_1 + 1$, $p_3 = 2, \alpha_2 = 2\alpha_1/(\alpha_1 + 1)$, and $d = \alpha_1 - 1$, Eq. (9.41) is satisfied. Moreover, selecting α_1 such that $0 < \alpha_1 < 1$ results in $d = \alpha_1 - 1 < 0$. Then, it can be concluded that Eq. (9.40) is homogeneous of degree $d = \alpha_1 - 1 < 0$. Notice that $\boldsymbol{h}(0) = 0$, from Eq. (9.40), and $\hat{\boldsymbol{h}}(0) = 0$ from Eqs. (9.37) to (9.38).

In order to prove the asymptotical stability of the equilibrium $\boldsymbol{y} = 0$ of the system Eq. (9.40), we propose the positive definite Lyapunov candidate function

$$V_2 = \frac{1}{\alpha_1 + 1}\sum_{i=1}^{n} k_{pi}|y_{1i}|^{\alpha_1 + 1} + \frac{1}{2}y_2^T M(q_d)y_2 + \frac{1}{2}(y_1 - y_3)^T(y_1 - y_3) \tag{9.42}$$

where y_{1i} denotes the ith component of vector y_1. The temporal derivative of Eq. (9.42) is

$$\dot{V}_2 = \dot{\boldsymbol{y}}_1^T K_p\,\mathrm{Sig}^{\alpha_1}(\boldsymbol{y}_1) + \boldsymbol{y}_2^T M(\boldsymbol{q}_d)\dot{\boldsymbol{y}}_2 + (\dot{\boldsymbol{y}}_1 - \dot{\boldsymbol{y}}_3)^T(\boldsymbol{y}_1 - \boldsymbol{y}_3) \tag{9.43}$$

where it was taken into account the fact that $\dot{M}(\boldsymbol{q}_d) = 0$ when $\boldsymbol{q}_d$ is constant. After substituting Eq. (9.40) in Eq. (9.43), we have

$$\dot{V}_2 = \boldsymbol{y}_2^T K_d\,\mathrm{Sig}^{\alpha_2}(\boldsymbol{y}_2) \tag{9.44}$$

By using Eq. (9.4) in Eq. (9.44), it can be concluded that $\dot{V}_2 \leq 0$, which implies that the origin is a stable equilibrium. By using the LaSalle invariance theorem (Kelly et al. 2005), the global asymptotical stability of the origin can be concluded.

Now consider the hyperbolic tangent function:

$$\mathrm{Tanh}(\varepsilon^{p_1}\boldsymbol{y}_1) = o(\varepsilon^{p_1}\boldsymbol{y}_1) \tag{9.45}$$

where $o(\varepsilon^{p_1}\boldsymbol{y}_1)$ means to be of order $\varepsilon^{p_1}\boldsymbol{y}_1$ as $\varepsilon^{p_1}\boldsymbol{y}_1 \to 0$. Therefore, for any fixed $\boldsymbol{y} = (\boldsymbol{y}_1^T\ \boldsymbol{y}_2^T\ \boldsymbol{y}_3^T)^T \in \Re^{3n}$, we have

$$\begin{aligned}\lim_{\varepsilon\to 0}\frac{\hat{\boldsymbol{h}}_1(\varepsilon^{p_1}\boldsymbol{y}_1, \varepsilon^{p_2}\boldsymbol{y}_2, \varepsilon^{p_3}\boldsymbol{y}_3)}{\varepsilon^{d+p_1}} &= -\alpha_0 \lim_{\varepsilon\to 0}\frac{\mathrm{Tanh}(\varepsilon^{p_1}\boldsymbol{y}_1)}{\varepsilon^{d+p_1}} \\ &= -\alpha_0 \lim_{\varepsilon\to 0} o(\varepsilon^{-d}\boldsymbol{y}_1) = 0\end{aligned} \tag{9.46}$$

Since $M^{-1}(\boldsymbol{y}_1 + \boldsymbol{q}_d)$ and $C(\boldsymbol{y}_1 + \boldsymbol{q}_d, \boldsymbol{y}_2)$ are smooth [see Hong et al. (2002); Su and Zheng (2009)], we obtain

$$\begin{aligned}&\lim_{\varepsilon\to 0} -\frac{M^{-1}(\varepsilon^{p_1}\boldsymbol{y}_1 + \boldsymbol{q}_d)}{\varepsilon^{d+p_2}}[(C(\varepsilon^{p_1}\boldsymbol{y}_1 + \boldsymbol{q}_d, \varepsilon^{p_2}\boldsymbol{y}_2 - \alpha_0\,\mathrm{Tanh}\,(\varepsilon^{p_1}\boldsymbol{y}_1)) \\ &\quad + F + k_{d0}\boldsymbol{I})(\varepsilon^{p_2}\boldsymbol{y}_2 - \alpha_0\,\mathrm{Tanh}(\varepsilon^{p_1}\boldsymbol{y}_1))] \\ &\quad = -M^{-1}(\boldsymbol{q}_d)[(C(\boldsymbol{q}_d, 0) + F + k_{d0}\boldsymbol{I}) \\ &\quad \times (\boldsymbol{y}_2 \lim_{\varepsilon\to 0}\varepsilon^{-d} - \alpha_0 \lim_{\varepsilon\to 0} o(\varepsilon^{p_1-d-p_2}\boldsymbol{y}_1))] = 0\end{aligned} \tag{9.47}$$

and

$$\begin{aligned}&\lim_{\varepsilon\to 0} -\frac{M^{-1}(\varepsilon^{p_1}\boldsymbol{y}_1 + \boldsymbol{q}_d)}{\varepsilon^{d+p_2}}[k_{p0}\varepsilon^{p_1}\boldsymbol{y}_1 + K_I(\varepsilon^{p_3}\boldsymbol{y}_3)] \\ &\quad = -M^{-1}(\boldsymbol{q}_d)\left[k_{p0}\boldsymbol{y}_1 \lim_{\varepsilon\to 0}\varepsilon^{p_1-d-p_2} - K_I\boldsymbol{y}_3 \lim_{\varepsilon\to 0}\varepsilon^{p_3-d-p_2}\right] = 0\end{aligned}$$

After applying the mean value theorem to each entry of $\widetilde{M}(y_1, q_d)$ yields

$$\widetilde{M}(\varepsilon^{p_1}\boldsymbol{y}_1, \boldsymbol{q}_d) = M^{-1}(\varepsilon^{p_1}\boldsymbol{y}_1 + \boldsymbol{q}_d) - M^{-1}(\boldsymbol{q}_d) = o(\varepsilon^{p_1}) \tag{9.48}$$

which results in

$$\begin{aligned}&\lim_{\varepsilon\to 0} -\frac{\widetilde{M}(\varepsilon^{p_1}\boldsymbol{y}_1, \boldsymbol{q}_d)\left\lfloor K_p\,\mathrm{Sig}^{\alpha_1}(\varepsilon^{p_1}\boldsymbol{y}_1) + K_d\,\mathrm{Sig}^{\alpha_2}(\varepsilon^{p_2}\boldsymbol{y}_2)\right\rfloor}{\varepsilon^{d+p_2}} \\ &\quad = \lim_{\varepsilon\to 0} o(\varepsilon^{p_1-d-p_2}) = 0\end{aligned} \tag{9.49}$$

Moreover, in virtue of a property of the ordinary hyperbolic secant function applied to Eq. (9.2), $\mathrm{Sech}^2(0) = I$. Then,

$$\lim_{\varepsilon\to 0} -\frac{\alpha_0(\mathrm{Sech}^2(\varepsilon^{p_1}\boldsymbol{y}_1)(\varepsilon^{p_2}\boldsymbol{y}_2 - \alpha_0\mathrm{Tanh}(\boldsymbol{y}_1)))}{\varepsilon^{d+p_2}} = \alpha_0\boldsymbol{y}_2 \lim_{\varepsilon\to 0}\varepsilon^{-d} - \alpha_0^2 \lim_{\varepsilon\to 0} o(\varepsilon^{p_1-d-p_2}\boldsymbol{y}_1) = 0 \tag{9.50}$$

where $p_3 - d - p_2 = p_1 - d - p_2 = 2(1-\alpha_1) > 0$ and $-d = 1 - \alpha_1 > 0$ for $0 < \alpha_1 < 1$. Then, for any fixed $\boldsymbol{y} = (\boldsymbol{y}_1^T\ \boldsymbol{y}_2^T\ \boldsymbol{y}_3^T)^T \in \Re^{3n}$, we have

$$\lim_{\varepsilon\to 0} \frac{\hat{\boldsymbol{h}}_2(\varepsilon^{p_1}\boldsymbol{y}_1, \varepsilon^{p_2}\boldsymbol{y}_2, \varepsilon^{p_3}\boldsymbol{y}_3)}{\varepsilon^{d+p_2}} = 0 \tag{9.51}$$

Thus, according to Lemma 1, the finite-time stability of the system Eq. (9.35) is proven. Moreover, by invoking Lemma 2, the global finite-time stability of the system Eq. (9.35) is proven.

9.4 Simulations

In order to show the feasibility of the proposed application of the finite-time regulation controller for a parallel manipulator, we carried out numerical simulations. Simulations of the finite-time nonlinear PID controller applied to the model of a real horizontal Five-Bar Mechanism were carried out.

9.4.1 Model of the Five-Bar Mechanism

A Five-Bar Mechanism is a planar parallel manipulator of two degrees of freedom. A scheme of the Five-Bar Mechanism is shown in Fig. 9.1. Notice that the structure of the mechanism is shown as an open structure. However, the extreme ends of the links 3 and 4 are joined. In the current section, the matrices $M'(\boldsymbol{\rho})$, $C'(\boldsymbol{\rho}, \dot{\boldsymbol{\rho}})$ of the model Eq. (9.10) and the matrices $M(\boldsymbol{q})$ Eq. (9.14), $C(\boldsymbol{q}, \dot{\boldsymbol{q}})$ Eq. (9.15) and $F(q)$ Eq. (9.17) of the model Eq. (9.19) (Soto and Campa 2014), including the transformation matrix $R(\boldsymbol{\rho})$ Eq. (9.12) and its temporal derivative, are shown. Note that since the Five-Bar Mechanism is horizontal, the gravitational forces vector is zero. The matrices of the model Eq. (9.10) are

$$M'(\boldsymbol{\rho}) = \begin{bmatrix} m'_{11} & 0 & m'_{13} & 0 \\ 0 & m'_{22} & 0 & m'_{24} \\ m'_{31} & 0 & m'_{33} & 0 \\ 0 & m'_{42} & 0 & m'_{44} \end{bmatrix}, C'(\boldsymbol{\rho}, \dot{\boldsymbol{\rho}}) = \begin{bmatrix} c'_{11} & 0 & c'_{13} & 0 \\ 0 & c'_{22} & 0 & c'_{24} \\ c'_{31} & 0 & 0 & 0 \\ 0 & c'_{42} & 0 & 0 \end{bmatrix}$$

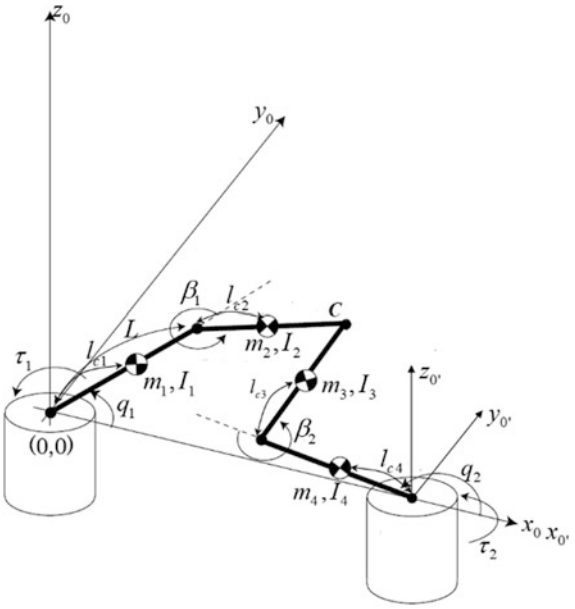

Fig. 9.1 Five-Bar Mechanism

where

$$
\begin{aligned}
m'_{11} &= m_1 l_{c1}^2 + m_3(L_1^2 + l_{c3}^2 + 2L_1 l_{c3}\ \cos(\beta_1)) + I_1 + I_3 \\
m'_{13} &= m_3(l_{c3}^2 + L_1 l_{c3}\ \cos(\beta_1)) + I_3 \\
m'_{31} &= m'_{13} \\
m'_{22} &= m_2 l_{c2}^2 + m_4(L_2^2 + l_{c4}^2 + 2L_2 l_{c4}\cos(\beta_2)) + I_2 + I_4 \\
m'_{24} &= m_4(l_{c4}^2 + L_2 l_{c4}\cos(\beta_2)) + I_4 \\
m'_{42} &= m'_{24} \\
m'_{33} &= m_3 l_{c3}^2 + I_3 \\
m'_{44} &= m_4 l_{c4}^2 + I_4
\end{aligned}
$$

and

$$
\begin{aligned}
c'_{11} &= -m_3 L_1 l_{c3}\sin(\beta_1)\dot{\beta}_1 \\
c'_{13} &= -m_3 L_1 l_{c3}\sin(\beta_1)(\dot{q}_1 + \dot{\beta}_1) \\
c'_{22} &= -m_4 L_2 l_{c4}\sin(\beta_2)\dot{\beta}_2 \\
c'_{24} &= -m_4 L_2 l_{c4}\sin(\beta_2)(\dot{q}_2 + \dot{\beta}_2) \\
c'_{31} &= m_3 L_1 l_{c3}\sin(\beta_1)\dot{q}_1 \\
c'_{42} &= m_4 L_2 l_{c4}\sin(\beta_2)\dot{\beta}_2
\end{aligned}
$$

The transformation matrix $R(\boldsymbol{\rho})$ and its temporal derivative $\dot{R}(\boldsymbol{\rho})$ are

$$R(\boldsymbol{\rho}) = \begin{bmatrix} 1 & 0 \\ 0 & 1 \\ r_{11} & r_{12} \\ r_{21} & r_{22} \end{bmatrix}, \dot{R}(\boldsymbol{\rho}) = \begin{bmatrix} 0 & 0 \\ 0 & 0 \\ \dot{r}_{11} & \dot{r}_{12} \\ \dot{r}_{21} & \dot{r}_{22} \end{bmatrix}$$

where

$$\begin{aligned} r_{11} &= -\frac{\sin(q_1 - q_2 - \beta_2)}{\sin(q_1 - q_2 + \beta_1 - \beta_2)} - 1 \\ r_{12} &= -\frac{\sin(\beta_2)}{\sin(q_1 - q_2 + \beta_1 - \beta_2)} \\ r_{21} &= \frac{\sin(\beta_1)}{\sin(q_1 - q_2 + \beta_1 - \beta_2)} \\ r_{22} &= -\frac{\sin(q_1 - q_2 - \beta_1)}{\sin(q_1 - q_2 + \beta_1 - \beta_2)} - 1 \end{aligned}$$

The matrices of the model Eq. (9.19) are

$$M(\boldsymbol{q}) = \begin{bmatrix} m_{11} & m_{12} \\ m_{21} & m_{22} \end{bmatrix} \quad C(\boldsymbol{q}, \dot{\boldsymbol{q}}) = \begin{bmatrix} c_{11} & c_{12} \\ c_{21} & c_{22} \end{bmatrix},$$

where

$$\begin{aligned} m_{11} &= m'_{44} r_{22}^2 + m'_{11} + m'_{13} r_{11} + r_{11}(m'_{13} + m'_{33} r_{11}) \\ m_{12} &= m'_{24} r_{21} + r_{12}(m'_{13} + m'_{33} r_{11}) + m'_{44} r_{21} r_{22} \\ m_{21} &= m'_{24} r_{21} + r_{12}(m'_{13} + m_{33} r_{11}) + m'_{44} r_{21} r_{22} \\ m_{22} &= m'_{33} r_{12}^2 + m'_{22} + m'_{24} r_{22} + r_{22}(m'_{24} + m'_{44} r_{22}) \end{aligned}$$

and

$$\begin{aligned} c_{11} &= c'_{11} + c'_{13} r_{11} + c'_{31} r_{11} + \dot{r}_{11}(m'_{13} + m'_{33} r_{11}) + m'_{44} r_{21} \dot{r}_{21} \\ c_{12} &= c'_{13} r_{12} + c'_{42} r_{21} + \dot{r}_{12}(m'_{13} + m'_{33} r_{11}) + m'_{44} r_{21} \dot{r}_{22} \\ c_{21} &= c'_{31} r_{12} + c'_{24} r_{21} + \dot{r}_{21}(m'_{24} + m'_{44} r_{22}) + m'_{33} r_{12} \dot{r}_{11} \\ c_{22} &= c'_{22} + c'_{24} r_{22} + c'_{42} r_{22} + \dot{r}_{22}(m'_{24} + m'_{44} r_{22}) + m'_{33} r_{12} \dot{r}_{12} \end{aligned}$$

The friction coefficients matrices of the model Eq. (9.10) and of the model Eq. (9.19) are

$$F' = \begin{bmatrix} f'_{11} & 0 & 0 & 0 \\ 0 & f'_{22} & 0 & 0 \\ 0 & 0 & f'_{33} & 0 \\ 0 & 0 & 0 & f'_{44} \end{bmatrix}, F = \begin{bmatrix} f_{11} & f_{12} \\ f_{21} & f_{22} \end{bmatrix}$$

where

$$f_{11} = f'_{11} + r_{11}^2 f'_{33} + r_{21}^2 f'_{44}$$
$$f_{12} = r_{11} r_{12} f'_{33} + r_{21} r_{22} f'_{44}$$
$$f_{21} = r_{11} r_{12} f'_{33} + r_{21} r_{22} f'_{44}$$
$$f_{22} = f'_{22} + r_{12}^2 f'_{33} + r_{22}^2 f'_{44}$$

The parameters of the dynamic model are shown in Table 9.1.

The elements of the matrix F of friction coefficients of the model Eq. (9.10) are shown in Table 9.2.

The desired values of the joint variables were computed using the inverse kinematic model [see Soto and Campa (2015)] based on the desired position of the end effector to reach a point $P_1 = (x_h - \Delta, y_h + \Delta)$ from the initial or home position $P_h = (x_h, y_h)$. Notice that $\Delta = 0.02$ (m). The coordinates of the initial position are $x_h = L_1$, $y_h = L_2$, with respect to the origin located at the rotation axis of the joint q_1 (see Fig. 9.1). The values of the joint variables that correspond to the home position are $q_1 = 0$ (rad) and $q_2 = 1.5708$ (rad), while the values that correspond to the point P_1 are $q_1 = 0.1686$ (rad) and $q_2 = 1.7441$ (rad). The gains and parameters of the finite-time nonlinear PID controller used in the simulations are shown in Table 9.3. These gains were selected by try and error procedure in order to achieve the best performance in terms of small position errors and at the same time, avoiding to exceed a maximum value of torque of 0.2 Nm. This maximum torque value is similar to the maximum values of electric motors that usually drive a small Five-Bar Mechanism for academic purposes.

Table 9.1 Parameters of the dynamic model of the Five-Bar Mechanism

Parameter	Value (units)	Parameter	Value (units)
L_1, L_2, L_3, L_4	0.127 (m)	m_2	0.121 (kg)
l_{c1}	0.047 (m)	m_3	0.085 (kg)
l_{c2}	0.045 (m)	m_4	0.063 (kg)
l_{c3}	0.069 (m)	I_1	0.0017 (kgm^2)
l_{c4}	0.062 (m)	I_2	0.0014 (kgm^2)
m_1	0.126 (kg)	I_4	8.74×10^{-5} (kgm^2)

Table 9.2 Friction parameters of the Five-Bar mechanism

Parameter	Value (units)
f'_{11}	0.01 (Nm/rad s)
f'_{22}	0.01 (Nm/rad s)
f'_{33}	0.00001 (Nm/rad s)
f'_{44}	0.00001 (Nm/rad s)

Table 9.3 Gains and parameters of the finite-time nonlinear PID controller

Gain	Joint 1	Joint 2	Units
k_{p0}	0.2	0.22	Nm/rad
k_{d0}	0.5	0.5	Nms/rad
K_p	0.37	0.36	Nm/rad
K_I	0.1	0.06	Nms/rad
K_d	0.1	0.01	Nm/rad
α_0	0.1	0.1	s^{-1}
α_1	0.5	0.5	(dimensionless)
α_2	0.6666	0.6666	(dimensionless)

Table 9.4 Gains of the nonlinear PID controller

Gain	Joint 1	Joint 2	Units
K_p	1.15	1.15	Nm/rad
K_d	0.5	0.5	Nms/rad
K_i	0.08	0.03	Nm/rads

For comparison purposed, simulations of a PID-like controller inspired in Kelly (1998) applied to the Five-Bar Mechanism were also conducted. The control law of this controller is

$$\boldsymbol{\tau} = -K_p\tilde{\boldsymbol{q}} - K_i \int_0^t \mathrm{Tanh}(\tilde{\boldsymbol{q}}(\sigma))\,\mathrm{d}\sigma - K_d\dot{\boldsymbol{q}}$$

The gains used for this controller are shown in Table 9.4. These gains were selected by try and test, in order to obtain the best performance of the controller and avoiding to exceed the maximum torque values.

9.4.2 Simulations Results

The results of the simulations are shown in Figs. 9.2, 9.3, 9.4, 9.5, 9.6 and 9.7. In Fig. 9.2, the position errors at joint 1 from both controllers, the finite-time nonlinear PID controller (FNPID) and the nonlinear PID from Kelly (1998), are shown. In Fig. 9.3, the position errors at joint 2 from both controllers are shown. From these figures, notice that the position errors of the FNPID in steady state are smaller than the position errors of the NPID. In Figs. 9.4 and 9.5, the commanded torques from the FNPID for joint 1 and joint 2, respectively, are shown. In Figs. 9.6 and 9.7, the commanded torques from the NPID for joint 1 and joint 2, respectively, are shown.

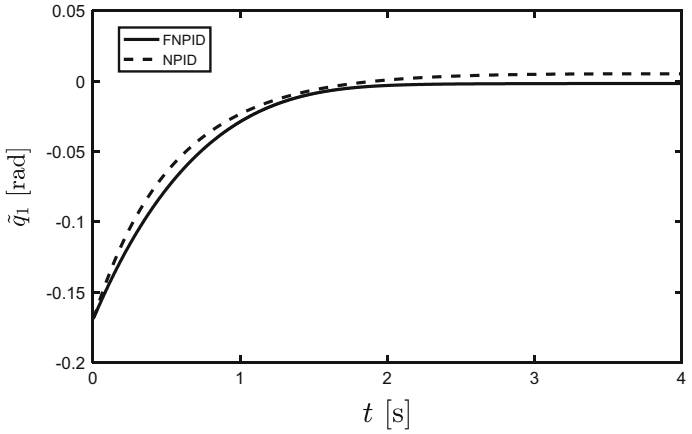

Fig. 9.2 Position errors in joint 1 from both controllers, FNPID and NPID

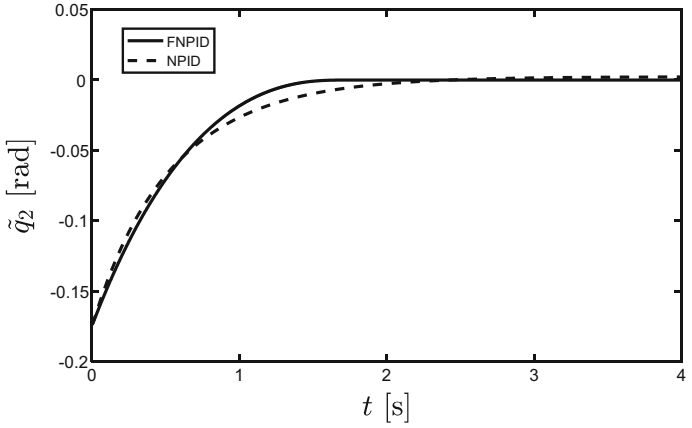

Fig. 9.3 Position errors in joint 2 from both controllers, FNPID and NPID

Notice that the torque signals from the NPID controller for both joints last longer times than the torque signals from the FNPID controller. This may imply smaller and shorter control efforts from the FNPID controller, which may result in improved durability of the drives and motors of the parallel machine. Notice that, as was pointed above, in the simulations we were careful in avoiding exceeding the maximum torque value of 0.2 (Nm).

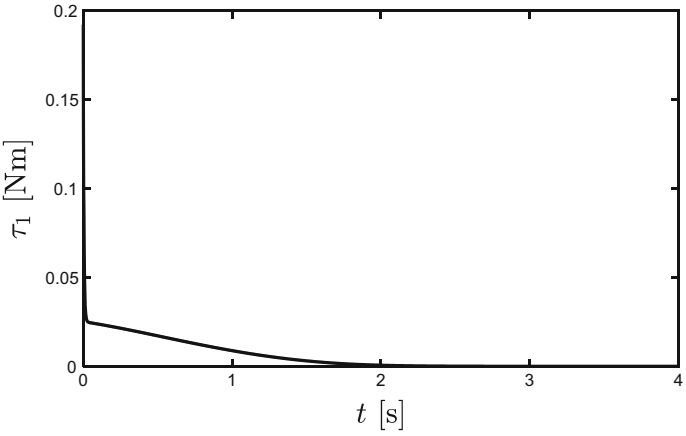

Fig. 9.4 Commanded torque from the FNPID controller, for joint 1

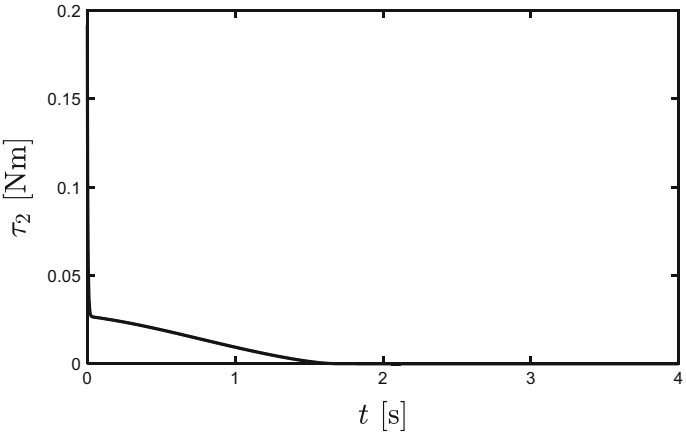

Fig. 9.5 Commanded torque from the FNPID controller, for joint 2

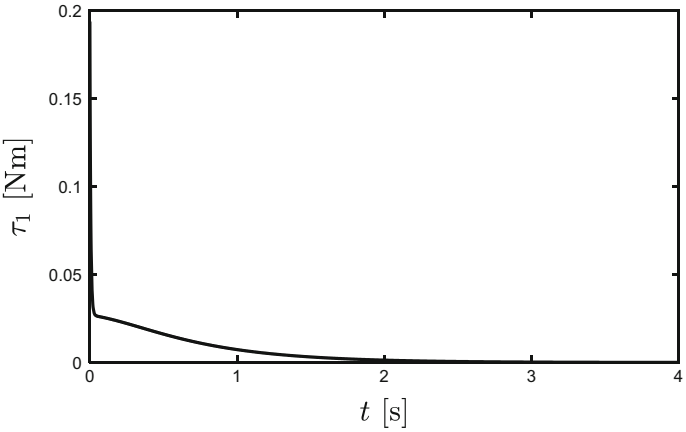

Fig. 9.6 Commanded torque from the NPID controller, for joint 1

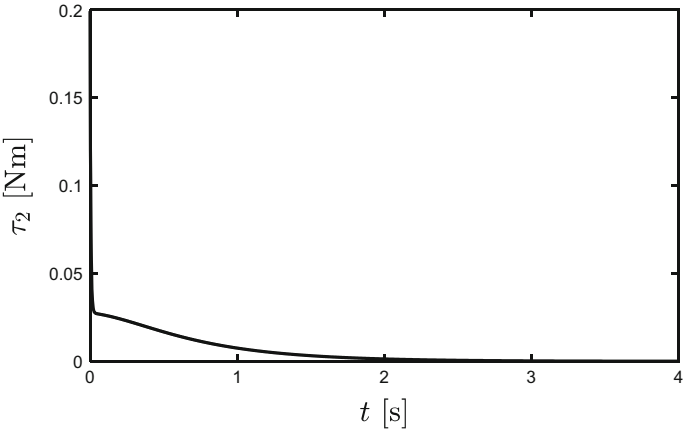

Fig. 9.7 Commanded torque from the NPID controller, for joint 2

9.5 Conclusion

In this work, we have reported the application of a finite-time nonlinear PID regulation controller to a Five-Bar Mechanism. The stability analysis of the system has been carried out, resulting in the global finite-time stability of the closed-loop system.

A dynamic model of a parallel robot, which is subject to mechanical constraints, has been obtained in structure similar to that of a serial robot. This let us analyze the closed-loop system in a similar way to analyzing a system with a serial robot.

Numerical simulations of the proposed controller applied to the model of a Five-Bar Mechanism were conducted. The simulations' results confirm the usefulness of the proposed approach.

References

Amato, F., De Tommasi, G., & Pironti, A. (2013). Necessary and sufficient conditions for finite-time stability of impulsive dynamical linear systems. *Automatica, 49*(8), 2546–2550.

Barnfather, J. D., Goodfellow, M. J., & Abram, T. (2017). Positional capability of a hexapod robot for machining applications. *The International Journal of Advanced Manufacturing Technology, 89*(1–4), 1103–1111. https://doi.org/10.1007/s00170-016-9051-0.

Bhat, S. P., & Bernstein, D. S. (1998). Continuous finite-time stabilization of the translational and rotational double integrators. *IEEE Transactions on Automatic Control, 43*(5), 678–682. https://doi.org/10.1109/9.668834.

Bhat, S. P., & Bernstein, D. S. (2000). Finite-Time stability of continuous autonomous systems. *SIAM Journal on Control and Optimization, 38*(3), 751–766. https://doi.org/10.1137/S0363012997321358.

Bhat, S. P., & Bernstein, D. S. (2005). Geometric homogeneity with applications to finite-time stability. *Mathematics of Control, Signals, and Systems, 17*(2), 101–127. https://doi.org/10.1007/s00498-005-0151-x.

Bourbonnais, F., Bigras, P., & Bonev, I. A. (2015). Minimum-time trajectory planning and control of a pick-and-place Five-Bar parallel robot. *IEEE/ASME Transactions on Mechatronics, 20*(2), 740–749. https://doi.org/10.1109/TMECH.2014.2318999.

Cheng, H., Yiu, Y-K., & Li, Z. (2003). Dynamics and control of redundantly actuated parallel manipulators. *IEEE/ASME Transactions on Mechatronics, 8*(4), 483–491.

Diaz-Rodriguez, M., Valera, A., Mata, V., & Valles, M. (2013). Model-based control of a 3-DOF parallel robot based on identified relevant parameters. *IEEE/ASME Transactions on Mechatronics, 18*(6), 1737–1744. https://doi.org/10.1109/TMECH.2012.2212716.

Dorato, P. (1961). Short time stability in linear time-varying systems. In *IRE International Convention Record* (pp. 83–87). USA: New York.

Enferadi, J., & Shahi, A. (2016). On the position analysis of a new spherical parallel robot with orientation applications. *Robotics and Computer-Integrated Manufacturing, 37,* 151–161. https://doi.org/10.1016/J.RCIM.2015.09.004.

Feng, Y., Yu, X., & Man, Z. (2002). Non-singular terminal sliding mode control of rigid manipulators. *Automatica, 38*(12), 2159–2167. https://doi.org/10.1016/S0005-1098(02)00147-4.

Ghorbel, F. H., Chetelat, O., Gunawardana, R., & Longchamp, R. (2000). Modeling and set point control of closed-chain mechanisms: theory and experiment. *IEEE Transactions on Control Systems Technology, 8*(5), 801–815. https://doi.org/10.1109/87.865853.

Gruyitch, L. T., & Kokosy, A. (1999). Robot control for robust stability with finite reachability time in the whole. *Journal of Robotic Systems*, *16*(5), 263–283. http://doi.org/10.1002/(SICI)1097-4563(199905)16:5<263::AID-ROB2>3.0.CO;2-Q.

Hong, Y., Xu, Y., & Huang, J. (2002). Finite-time control for robot manipulators. *Systems & Control Letters, 46*(4), 243–253. https://doi.org/10.1016/S0167-6911(02)00130-5.

Huang, Z., & Cao, Y. (2005). Property identification of the singularity loci of a class of Gough-Stewart manipulators. *The International Journal of Robotics Research, 24*(8), 675–685. https://doi.org/10.1177/0278364905054655.

Kelaiaia, R. (2017). Improving the pose accuracy of the Delta robot in machining operations. *The International Journal of Advanced Manufacturing Technology, 91*(5–8), 2205–2215. https://doi.org/10.1007/s00170-016-9955-8.

Kelly, R. (1998). Global positioning of robot manipulators via PD control plus a class of nonlinear integral actions. *IEEE Transactions on Automatic Control, 43*(7), 934–938. https://doi.org/10.1109/9.701091.

Kelly, R., Santibáñez, V., & Loría, A. (Antonio). (2005). *Control of robot manipulators in joint space*. Berlin: Springer.

Khalil, W. (Wisama), & Dombre, E. (Etienne). (2004). *Modeling, identification and control of robots*. Kogan Page Science.

Khan, W. A., Krovi, V. N., Saha, S. K., & Angeles, J. (2005). Recursive kinematics and inverse dynamics for a planar 3R parallel manipulator. *Journal of Dynamic Systems, Measurement, and Control, 127*(4), 529. https://doi.org/10.1115/1.2098890.

Li, Q., Wu, W., Xiang, J., Li, H., & Wu, C. (2015). A hybrid robot for friction stir welding. *Proceedings of the Institution of Mechanical Engineers, Part C: Journal of Mechanical Engineering Science, 229*(14), 2639–2650. https://doi.org/10.1177/0954406214562848.

Michel, A. (1970). Quantitative analysis of simple and interconnected systems: Stability, boundedness, and trajectory behavior. *IEEE Transactions on Circuit Theory, 17*(3), 292–301. https://doi.org/10.1109/TCT.1970.1083119.

Muller, A. (2005). Internal preload control of redundantly actuated parallel manipulators—Its application to backlash avoiding control. *IEEE Transactions on Robotics, 21*(4), 668–677. https://doi.org/10.1109/TRO.2004.842341.

Nan, R., Li, D., Jin, C., Wang, Q., Zhu, L., Zhu, W., … Qian, L. (2011). The Five-Hundred-Meter Aperture Spherical Radio Telescope (FAST) Project. *International Journal of Modern Physics D*, *6,* 989–1024. http://doi.org/10.1142/S0218271811019335.

Pierrot, F., Reynaud, C., & Fournier, A. (1990). DELTA: a simple and efficient parallel robot. *Robotica, 8*(2), 105. https://doi.org/10.1017/S0263574700007669.

Polyakov, A. (2014). Stability notions and Lyapunov functions for sliding mode control systems. *Journal of the Franklin Institute, 351*(4), 1831–1865. https://doi.org/10.1016/J.JFRANKLIN.2014.01.002.

Polyakov, A., & Poznyak, A. (2009). Lyapunov function design for finite-time convergence analysis: "Twisting" controller for second-order sliding mode realization. *Automatica, 45*(2), 444–448. https://doi.org/10.1016/J.AUTOMATICA.2008.07.013.

Ren, L., Mills, J. K., & Sun, D. (2007). Experimental comparison of control approaches on trajectory tracking control of a 3-DOF parallel robot. *IEEE Transactions on Control Systems Technology, 15*(5), 982–988. https://doi.org/10.1109/TCST.2006.890297.

Salinas, A., Moreno-Valenzuela, J., & Kelly, R. (2016). A family of nonlinear PID-like regulators for a class of torque-driven robot manipulators equipped with torque-constrained actuators. *Advances in Mechanical Engineering, 8*(2), 168781401662849. https://doi.org/10.1177/1687814016628492.

Soto, I., & Campa, R. (2014). On dynamic modelling of parallel manipulators: The Five-Bar mechanism as a case study. *International Review on Modelling and Simulations (IREMOS)*, *7*(3), 531–541. http://doi.org/10.15866/IREMOS.V7I3.1899.

Soto, I., & Campa, R. (2015). Modelling and control of a spherical inverted pendulum on a five-bar mechanism. *International Journal of Advanced Robotic Systems, 12*(7), 95. https://doi.org/10.5772/60027.

Su, Y., & Zheng, C. (2017). PID control for global finite-time regulation of robotic manipulators. *International Journal of Systems Science, 48*(3), 547–558. https://doi.org/10.1080/00207721.2016.1193256.

Weiss, L., & Infante, E. (1967). Finite time stability under perturbing forces and on product spaces. *IEEE Transactions on Automatic Control, 12*(1), 54–59. https://doi.org/10.1109/TAC.1967.1098483.

Wu, H., Handroos, H., & Pessi, P. (2008). Mobile parallel robot for assembly and repair of ITER vacuum vessel. *Industrial Robot: An International Journal, 35*(2), 160–168. https://doi.org/10.1108/01439910810854656.

Xie, F., & Liu, X.-J. (2016). Analysis of the kinematic characteristics of a high-speed parallel robot with Schönflies motion: Mobility, kinematics, and singularity. *Frontiers of Mechanical Engineering, 11*(2), 135–143. https://doi.org/10.1007/s11465-016-0389-7.

Yu, S., Yu, X., Shirinzadeh, B., & Man, Z. (2005). Continuous finite-time control for robotic manipulators with terminal sliding mode. *Automatica, 41*(11), 1957–1964. https://doi.org/10.1016/J.AUTOMATICA.2005.07.001.

Su, Y., & Zheng, C. (2009). A simple nonlinear PID control for finite-time regulation of robot manipulators. In *2009 IEEE International Conference on Robotics and Automation* (pp. 2569–2574). IEEE. http://doi.org/10.1109/ROBOT.2009.5152244.

Su, Y., & Zheng, C. (2010). A simple nonlinear PID control for global finite-time regulation of robot manipulators without velocity measurements. In *2010 IEEE International Conference on Robotics and Automation* (pp. 4651–4656). IEEE. http://doi.org/10.1109/ROBOT.2010.5509163.

Zhao, D., Li, S., Zhu, Q., & Gao, F. (2010). Robust finite-time control approach for robotic manipulators. *IET Control Theory and Applications, 4*(1), 1–15. https://doi.org/10.1049/iet-cta.2008.0014.